# Metastable and unstable hydrodynamics in multiphase lattice Boltzmann

Matteo Lulli,[1,2,*] Luca Biferale,[3] Giacomo Falcucci,[4,5] Mauro Sbragaglia,[3] Dong Yang,[1] and Xiaowen Shan[1,6,†]

[1]*Department of Mechanics and Aerospace Engineering, Southern University of Science and Technology, Shenzhen, Guangdong 518055, China*

[2]*Department of Physics, The Chinese University of Hong Kong, Sha Tin, Hong Kong, China*

[3]*Department of Physics and INFN, University of Rome "Tor Vergata", Via della Ricerca Scientifica 1, 00133 Rome, Italy*

[4]*Department of Enterprise Engineering "Mario Lucertini", University of Rome "Tor Vergata", Via del Politecnico 1, 00133 Rome, Italy*

[5]*John A. Paulson School of Engineering and Applied Physics, Harvard University, 33 Oxford Street, 02138 Cambridge, Massachusetts, USA*

[6]*Institute of Advanced Study, BNU-HKBU United International College, Zhuhai, Guangdong 519088, China*

(Received 15 December 2022; revised 22 December 2023; accepted 3 January 2024; published 15 April 2024)

Metastability in liquids is at the foundation of complex phase transformation dynamics such as nucleation and cavitation. Intermolecular interaction details, beyond the equation of state, and thermal hydrodynamic fluctuations play a crucial role. However, most numerical approaches suffer from a slow time and space convergence, thus hindering the convergence to the hydrodynamic limit. This work shows that the Shan-Chen lattice Boltzmann model has the unique capability of simulating the hydrodynamics of the metastable state. The structure factor of density fluctuations is theoretically obtained and numerically verified to a high precision, for all simulated wave vectors, reduced temperatures, and pressures, deep into the metastable region. Such remarkable agreement between the theory and simulations leverages the exact implementation at the lattice level of the mechanical equilibrium condition. The static structure factor is found to consistently diverge as the temperature approaches the critical point or the density approaches the spinodal line at a subcritical temperature. Theoretically predicted critical exponents are observed in both cases. Finally, the phase separation in the unstable branch follows the same pattern, i.e., the generation of interfaces with different topology, as observed in molecular dynamics simulations.

DOI: 10.1103/PhysRevE.109.045304

## I. INTRODUCTION

Metastability constitutes one of the basic mechanisms for cavitation inception and nucleation in general [1,2] which are of paramount importance in both fundamental science and critical applications such as sono-luminescence, hydrogen nucleation on the electrodes of electrolysis cells, flow around underwater propeller blades, and jet break-up dynamics [3]. In contrast to *spinodal decomposition* where the initial state is thermodynamically unstable and phase separation occurs immediately in response to infinitesimal extensive perturbations [1], *nucleation* is associated with the transition from a metastable state to a more stable one which can be far apart on the phase diagram. To phase-separate, a localized, finite-amplitude perturbation is required to overcome the energy barrier of forming a critical-size gas/liquid embryo. While in the more common heterogeneous nucleation, initial inhomogeneities are present due to natural impurities such as gas pockets and solid particles, in homogeneous nucleation [4] the dynamics of nucleation is the result of the competition between thermal fluctuations and the energy barrier which is the characteristic of metastable states.

Several physical properties come into play influencing nucleation and cavitation, namely, (i) hydrodynamic thermal fluctuations, (ii) the surface tension between different phases, and (iii) the cost of formation of a critical size gas/liquid embryo able to overcome the nucleation free-energy barrier. These properties are typically addressed in (i) the stochastic hydrodynamic approach [5], (ii) the thermodynamics of multiphase interfaces [6], and (iii) classical nucleation theory (CNT) [1,2]. Computer simulations of nucleation are commonly conducted using molecular dynamics (MD), which can treat a limited number of particles, approaching the hydrodynamic limit only at very high computational cost. Recently, homogeneous and heterogeneous nucleation in the presence of fluctuating hydrodynamics has been considered in the context of finite-difference methods yielding interesting results [7,8] that showcased the technical advantages of mesoscopic models over MD approaches [8]. However, the characteristics of metastability, i.e., a local equilibrium that can withstand infinitesimal perturbation, can be addressed only near the critical point while bringing into the picture slow-relaxing modes for small wave vectors, $k \sim 0$ [7,8], i.e., a slow hydrodynamic response to thermal fluctuations. The model has been shown to be able to describe water under large tension [9]; however, a study of the fluctuations across different length scales in such a metastable regime is still missing.

Other mesoscopic approaches could be considered for the modeling of a metastable hydrodynamic state, such as *dissipative particle dynamics* (DPD) or *density functional theory* (DFT). However, while enforcing momentum conservation, DPD implements random forces in a very specific way hindering its connection to the fluctuating hydrodynamics stress tensor [5]. Finally, DFT has been extended

*mlulli@phy.cuhk.edu.hk

†xiaowenshan@uic.edu.cn

 

to the description of dynamic phenomena close to equilibrium, i.e., diffusion and the recovery of Euler equation [10], while the direction of stochastic hydrodynamics is yet to be explored.

The mesoscopic lattice Boltzmann method (LBM) has achieved significant success in hydrodynamic simulations [11,12]. In this paper we demonstrate the ability of Shan-Chen (SC) lattice Boltzmann model (LBM) [13,14] to correctly capture metastable and unstable hydrodynamics through a coherent inclusion of the stochastic stress tensor [5]. In the unstable region of the phase diagram, immediate phase separation is observed for very small amplitude perturbations, which follows the same pattern observed in molecular dynamics simulations [15], i.e., reaching in the final stage interfaces with different topology as a function of the initial density. In the metastable region phase separation occurs on a timescale that diverges as the noise amplitude goes to zero. The system response to thermal fluctuations is studied by means of a stochastic hydrodynamics approach [5,16,17]. The structure factor (or form factor), $S(k)$, which converges to the isothermal compressibility in the long-wavelength limit, is obtained theoretically and verified numerically to a high precision: due to the exact implementation of the mechanical equilibrium condition on the lattice [18,19], an *exact* expression for $S(k)$ is obtained (see Appendix B 2). Two different scaling regimes of $S(k)$ are probed: (i) w.r.t. the temperature difference with critical point along the equilibrium binodal curve, and (ii) w.r.t. pressure difference with the spinodal values along an isotherm in the metastable region. A very good convergence, driven by the hydrodynamic response to thermal fluctuations, is observed over four to five decades in both reduced temperature and pressure. In both cases the compressibility is found to diverge with exponent values in agreement with theoretical predictions [1]. The paper is organized as follows: In Sec. II we introduce the Shan-Chen multiphase model equation of state in nondimensional form and derive the scaling properties of the isothermal compressibility approaching the critical and spinodal points; further, after the introduction of hydrodynamic fluctuations, we derive the exact form of the static density structure factor starting from the expression of the lattice pressure tensor; next in. Sec. III we present the simulations results for the scaling of the isothermal compressibility near the critical and spinodal points for all accessible wavevectors as well as the sequence of final interfaces obtained in the unstable region from a homogeneous initial condition; discussions and conclusions follow in Sec. IV. All the numerical results in this paper can be independently reproduced by means of a GPU/CPU implementation, which can be found on the GitHub repository of the "idea.deploy" framework [20–27].

## II. MODEL PROPERTIES

### A. Scaling regimes

LBM originated from a lattice-gas fluid model [11,12] and later reformulated as a special velocity-space discretization of the Boltzmann equation. The single-particle distribution function, $f(\boldsymbol{x}, \boldsymbol{\xi}, t)$, is simplified to its values on a small set of discrete velocities while preserving the dynamics of its moments, and hence the hydrodynamics [28,29]. The SC non-ideal-gas model incorporates the interparticle interaction through a mean-field Vlasov force

$$\boldsymbol{F}(\boldsymbol{x}) = G\psi(\boldsymbol{x}) \sum_{a=1}^{N_F} w(|\boldsymbol{e}_a|^2)\psi(\boldsymbol{x}+\boldsymbol{e}_a)\boldsymbol{e}_a, \tag{1}$$

where $G > 0$ is an interaction strength, $\{\boldsymbol{e}_a : a = 1, \ldots, N_F\}$ the vectors pointing from $\boldsymbol{x}$ to its interacting neighbors on the lattice, $w(|\boldsymbol{e}_a|^2)$ a set of weights, and $\psi(\boldsymbol{x})$ the so-called pseudo-potential encapsulating the details of interaction over fixed distances. Together with the symmetry of the interacting set, the carefully chosen weights, $w(|\boldsymbol{e}_a|^2)$, ensure macroscopic isotropy [19,30,31].

The interaction alters the equation of state (EoS) by adding a non-ideal-gas contribution to the pressure, yielding the following non-ideal-gas EoS:

$$p(n, T) = nk_BT - \frac{G}{2}\psi^2(n), \tag{2}$$

where $n$ and $T$ are respectively the number density and absolute temperature. Although the original model [13] was defined for an isothermal underlying LB model, the above EoS can be easily verified in thermal models.

We first show that the iso-thermal compressibility, $\kappa_T \equiv n^{-1}\partial n/\partial p$, obtained from Eq. (2) diverges with the correct exponents [1] as the system approaches from a stable configuration to the critical point ($T/T_c \to 1$), or the spinodal curve ($n \to n_s$). In the present study, $\psi$ is set to $\exp(-1/n)$ [14]. Introducing two scaling constants, $a$ and $b$, such that $\psi = a\exp(-b/n)$, the EoS becomes

$$p = nk_BT - \frac{Ga^2}{2}\exp\left(-\frac{2b}{n}\right). \tag{3}$$

As $a^2$ also regulates the interaction strength, $G$ is omitted hereinafter to remove the redundancy. Letting the critical density, temperature, and pressure be denoted by $n_c$, $T_c$ and $p_c$ respectively and using the conditions $\partial p/\partial n = \partial^2 p/\partial n^2 = 0$ at the critical point, we can solve $a$ and $b$ in terms of $n_c$ and $T_c$ as

$$a = e\sqrt{k_BT_cn_c} \quad \text{and} \quad b = n_c. \tag{4}$$

$\psi$ and the EoS are then expressed in critical quantities as

$$\psi(n) = \sqrt{k_BT_cn_c}\exp\left(1 - \frac{n_c}{n}\right), \tag{5}$$

$$p = nk_BT - \frac{n_ck_BT_c}{2}\exp\left(2 - \frac{2n_c}{n}\right). \tag{6}$$

The critical pressure is equal to $p_c \equiv p(n_c, T_c) = n_ck_BT_c/2$. In terms of the *reduced* quantities: $\hat{n} = n/n_c$, $\hat{p} = p/p_c$, and $\hat{T} = T/T_c$, the EoS becomes

$$\hat{p} = 2\hat{n}\hat{T} - \exp(2 - 2/\hat{n}). \tag{7}$$

It is useful also to redefine the pseduo-potential in the nondimensional form as $\psi(n) = \exp(1 - \hat{n}^{-1})$ so that the EoS can be rewritten in the form $\hat{p} = 2\hat{n}\hat{T} - \psi^2$. This convention is adopted for the equations below. The rescaled EoS, known as the *general EoS*, has identical shape as the unscaled one but a critical point at $\hat{n} = \hat{p} = \hat{T} = 1$. The phase diagram is shown in Fig. 1.

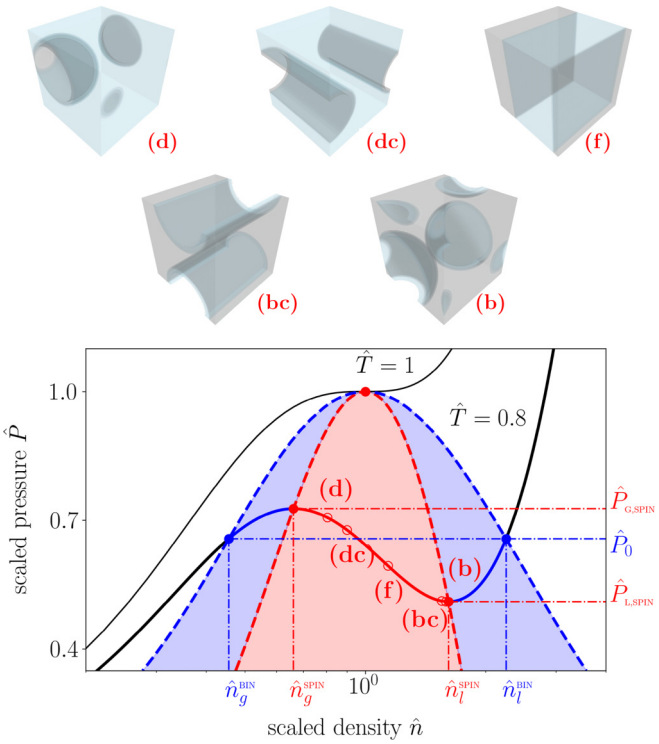


FIG. 1. Lower panel: Isotherms at the critical temperature ($\hat{T}=1$) and subcritical temperature of $\hat{T}=0.8$. Dashed blue and red (darker and lighter shades) lines are respectively the binodal and spinodal curves, and the blue- and red-shaded areas (darker and lighter shades) the metastable and unstable regions. The five points on the unstable part of the isotherm (red solid line) correspond to the initial densities which phase separate immediately with final interface topologies of droplet (d), droplet-cylinder (dc), flat (f), bubble-cylinder (bc), and bubble (b), all shown in the upper panel.

By taking the inverse of the derivative $\partial/\partial\hat{n}$ of Eq. (7), we have nondimensionalized compressibility

$$\hat{\kappa}_T = \frac{\hat{n}}{2}\left[\hat{n}^2\hat{T} - \exp\left(2-\frac{2}{\hat{n}}\right)\right]^{-1}. \tag{8}$$

Since $\hat{n}\cong 1$ near critical point, $\hat{\kappa}_T \sim (\hat{T}-1)^{-1}$ as $\hat{T}\to 1$. Now consider a point, $(\hat{p}_s,\hat{n}_s)$, on the spinodal curve. Using the fact that $\partial\hat{p}/\partial\hat{n}=0$, the leading-order expansion in the vicinity is

$$\hat{p}-\hat{p}_s \cong \frac{1}{2}\left.\frac{\partial^2\hat{p}}{\partial\hat{n}^2}\right|_{\hat{n}=\hat{n}_s,\hat{T}} (\hat{n}-\hat{n}_s)^2. \tag{9}$$

Denoting $A=\partial^2\hat{p}/\partial\hat{n}^2|_{\hat{n}=\hat{n}_s,\hat{T}}$ for brevity, we have

$$\hat{\kappa}_T \cong \frac{1}{A\hat{n}_s}(\hat{n}-\hat{n}_s)^{-1} \cong \frac{1}{\sqrt{2A\hat{n}_s}}(\hat{p}-\hat{p}_s)^{-1/2}. \tag{10}$$

Equations (8) and (10) yield the critical and spinodal scaling of $\hat{\kappa}_T$, respectively, which will be shown below to match the correlation function of the density fluctuations in the long-wavelength limit.

### B. Fluctuating hydrodynamics and structure function

We now discuss the phase separation as a response to thermal fluctuations. In the Landau hydrodynamic fluctuation theory [5], thermal fluctuations are included into hydrodynamics by the "outside" [5] Langevin-type noise stress, $\boldsymbol{R}$,

$$\partial_t n + \nabla\cdot(n\boldsymbol{u}) = 0, \tag{11a}$$

$$\partial_t(n\boldsymbol{u}) + \nabla\cdot(n\boldsymbol{u}\boldsymbol{u}) = -\nabla\cdot\boldsymbol{P} + \nabla\cdot\boldsymbol{\sigma} + \nabla\cdot\boldsymbol{R}, \tag{11b}$$

$$\boldsymbol{\sigma} = \mu_s\left[\nabla\boldsymbol{u} + (\nabla\boldsymbol{u})^T - \frac{2}{D}\boldsymbol{I}\nabla\cdot\boldsymbol{u}\right] + \mu_b\boldsymbol{I}\nabla\cdot\boldsymbol{u}. \tag{11c}$$

where $\boldsymbol{u}$ is the fluid velocity, $\boldsymbol{\sigma}$ is the Newtonian deviatoric stress, $\boldsymbol{P}$ the pressure tensor containing both the hydrostatic term and the one due to intermolecular interaction which vanishes in the ideal-gas limit, $\mu_s$, $\mu_b$ are the shear/bulk viscosity, respectively, and $D$ the space dimensionality. $\boldsymbol{R}$ is a spatially and temporally uncorrelated Gaussian random stress with variance proportional to the *hydrodynamic fluctuations energy* $k_B\vartheta$ where $k_B \simeq 1.380649\times 10^{-23}$ (J/K) (for more details see Appendix B 1). We are working in the isothermal framework for which the background temperature is constant and fluctuations enter only through the stress tensor [16,17]. It would be very interesting to extend the present approach by including the heat current as already proposed in the general theory. A framework for including thermal fluctuation in LBM was developed by adding noise terms to the LBM equation [16,17]

$$f_i(\boldsymbol{x}+\boldsymbol{\xi}_i, t+1) - f_i(\boldsymbol{x},t) = \Omega_i(f_i) + F_i + \eta_i, \tag{12}$$

where $\Omega$ is the usual Bhatnagar-Gross-Krook (BGK) collision term [11,12] giving rise to the Navier-Stokes hydrodynamics. $\eta_i$ is the Langevin-type noise with a covariance matrix diagonal in the moment space assuring the local conservation of the hydrodynamic moments [16,17]. $F_i$ is the forcing term [32] used to implement Eq. (1). We now turn our attention to the structure function $\bar{S}(k)=\langle|\delta\bar{n}(k)|^2\rangle$, with the angle brackets $\langle\cdots\rangle$ indicating the steady state average. This is the Fourier transform of the density correlation function connected to the direct pair correlation function at the foundation of Ornstein-Zernike theory [16,17]. The structure factor can be directly measured in experiments and compared with simulations data [33], hence a relevant quantity proportional to the isothermal compressibility $\kappa_T$ in the long-wavelength limit, $\bar{S}(0)\sim\kappa_T$ [34]. This allows us to assess the robustness of the simulations by studying the two scaling limits discussed above, i.e., in temperature towards the critical and pressure towards the spinodal points. To calculate $\bar{S}(k)$ we start from the Fourier transform of the Navier-Stokes equations [16,17] linearized around the quiescent homogeneous state $\langle n\rangle = n_0$ and $\boldsymbol{u}=\delta\boldsymbol{u}$,

$$\partial_t\delta\bar{n} = \imath n_0 k\delta\bar{u}_{||},$$

$$\partial_t\delta\bar{u}_{||} = \frac{\imath k}{n_0}(\delta\bar{P}_{||} - \hat{R}_{||}) - \nu_{||}k^2\delta\bar{u}_{||}, \tag{13}$$

where $u_{||}=\boldsymbol{u}\cdot\hat{\mathbf{k}}$, $\nu_{||}=\nu_{\mathrm{b}}+2(1-1/D)\nu_{\mathrm{s}}$ is the longitudinal viscosity and $\bar{R}_{||}=\bar{\boldsymbol{R}}:\hat{\mathbf{k}}\hat{\mathbf{k}}$. The key quantity is $\delta\bar{P}_{||}=\delta\bar{\boldsymbol{P}}:\hat{\mathbf{k}}\hat{\mathbf{k}}=\bar{c}_s^2(k)\delta\bar{n}$, defining the $k$-dependent speed of sound [16,17] $\bar{c}_s^2(k)$. For the SC model there exist a lattice expression for the pressure tensor which enjoys an important property for flat interfaces: The normal component is constant

to machine precision throughout the interface thus realizing the mechanical equilibrium condition $\hat{P}_N = \hat{P}_0$ *on the lattice* [19,30] (see Appendix B 2). One can notice that the variation of the longitudinal component of the pressure tensor is actually proportional to $\hat{P}_N$ given that $\hat{\mathbf{k}}$ is in the direction of the density gradient, hence one can leverage the one-dimensional expression

$$\hat{P}_N(x) = 2\hat{n}(x)\hat{T} - \tfrac{1}{2}\psi(x)[\psi(x+1) + \psi(x-1)]. \quad (14)$$

As detailed in the Appendix B 2 one can take the variation of (B10) as $\delta\hat{P}_N = d\hat{P}_N/d\hat{n}|_{\hat{n}_0}\delta\hat{n}$, take its Taylor expansion in real space and finally its Fourier transform. By virtue of the definition of $\hat{P}_N$ it is possible to sum the series in $k$ and obtain for the scale-dependent speed of sound

$$\hat{c}_s^2(k) = \hat{c}_{s,0}^2 - \psi_0\psi_0'[\cos(k) - 1], \quad (15)$$

where $\hat{c}_{s,0}^2 = d\hat{p}/d\hat{n} = 2\hat{T} - 2\psi_0\psi_0'$ (see Eq. (6)). This result simply follows from the fact that Eq. (B10) is closely related to the lattice Laplacian [35,36]. It is possible to combine the two Eqs. (13) and obtain a second-order equation in time for $\delta\hat{n}$, which can be again Fourier transformed in the frequency domain and yield an algebraic expression for $\delta\hat{n}(\boldsymbol{k}, \omega)$. Hence, one defines the nondimensional dynamic structure factor as $\hat{S}(\mathbf{k}\Delta x, \omega\Delta t) = \langle|\delta\hat{n}(\mathbf{k}\Delta x, \omega\Delta t)|^2\rangle$, where $\Delta x$ and $\Delta t$ are some characteristic space and time lengths. The frequency dependence can be integrated out by considering a complex contour integral around the poles yielding the nondimensionalized structure factor $\hat{S}(k\Delta x) = 2\hat{n}_0\hat{\vartheta}/n_c\hat{c}_s^2(k\Delta x)$,

$$\hat{S}(k\Delta x) = \frac{2\hat{n}_0\hat{\vartheta}}{n_c\left\{\hat{c}_{s,0}^2 - \psi_0\psi_0'[\cos(k\Delta x) - 1]\right\}}, \quad (16)$$

where $\psi_0 = \psi(n_0)$, $\psi' = d\psi/dn$ and $\hat{\vartheta} = \vartheta/T_c$. We remark that this expression is an exact identity valid for all values of $k$ and $\hat{T}$ in contrast to the previous approaches [7,8,16,17], which are limited to $O(k^2)$ and reliable only near the critical point. Finally we remark on the similarity of Eq. (16) to the momentum space propagator of the lattice Gaussian model [36] (see Appendix B 2 for details).

## III. RESULTS

To include hydrodynamic fluctuations in simulation, we extended [16,17] to three dimensions (3D). Key to the implementation is a proper choice of the covariance matrix for the noise populations $\eta_i$. As observed in [17], one needs to consider only a diagonal correlation matrix in the space of the noise hydrodynamic moments $N_a$ which are obtained by some specific linear combinations of the noise populations, i.e., $N_a = \sum_i m_{ai}\eta_i$, hence $\Xi_{ab} = \langle N_a N_b\rangle \propto k_B\vartheta\delta_{ab}$ with $a > 3$. The covariance of the first four moments, $a = 0, 1, 2, 3$, are set to zero to ensure mass and momentum conservation.

We performed two kinds of simulations in periodic 3D domains of linear size $L$ with homogeneous density $n_0$ as initial condition: (i) $n_0$ is chosen along the isotherm $\hat{T} = 0.8$ in the unstable region with the fluctuations energy set to $k_B\vartheta = 10^{-10}$ (lbu) [37], and (ii) $n_0$ belongs to either the liquid or the gas phases along (a) the isotherm $\hat{T} = 0.8$ in the metastable region approaching the spinodal points or (b) along the binodal approaching the critical point while keeping

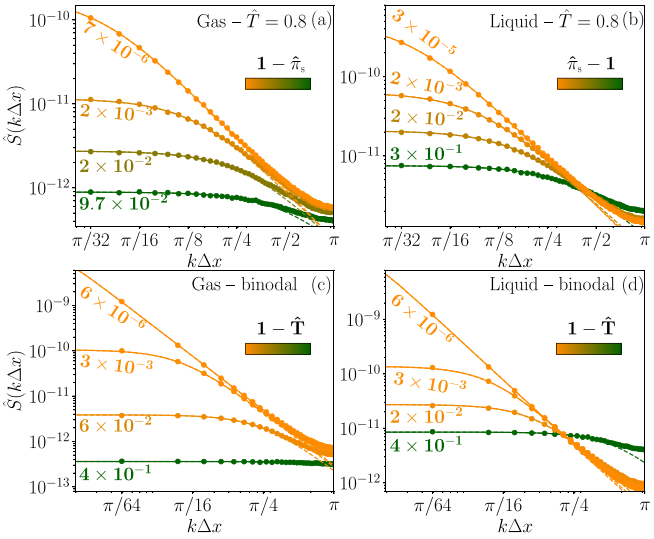


FIG. 2. Density structure factor $S(k)$ as a function of $k$ at varying pressure along the $\hat{T} = 0.8$ isotherm (top row) and at varying temperature along the binodal (bottom row). The left and right columns show the cases starting from the gas and liquid phase respectively. The color scale, from green to orange (lighter to darker shade), indicates the distance in pressure from the spinodal line or in temperature from the critical point, with the values reported near the corresponding curve. In dashed lines we report Eq. (16) truncated at $O(k^2)$.

$k_B\vartheta = 10^{-13}$ (lbu) in order to avoid nucleation. In the upper panels of Fig. 1 we report the final density configurations in the unstable region: Our simulations display qualitative the same sequence of interface shapes as in [38]. Indeed, the MD simulations and the present LBM approach share the main symmetry feature of exact mass conservation. This results can be used to estimate the curvature dependence of the surface tension [38]: The connection with the recently proposed SC lattice Boltzmann approach for the estimation of the Tolman length [39,40] will be the subject of a future work.

Shown in Figs. 2 and 3 are the numerically measured structure factor together with the values of Eq. (16). We note that the finite simulation domains of $L = 128$ and $L = 512$ impose an artificial minimum wave number of approximately $10^{-3}$. A number of interesting aspects are to be seen. First, in contrast to previous results [17], numerical measurements are in excellent agreement with the exact expression across several decades of wave length and distance from the critical and spinodal line. For comparison, Eq. (16) truncated to $O(k^2)$ is also shown as the thin dashed lines: the agreement worsens for $k \gtrsim \pi/2$. Second, the scaling at both $\hat{\pi}_s = \hat{P}/\hat{P}_s \to 1$ and $\hat{T} \to 1$ in Figs. 2 and 3 indicate the diverging trends of $\kappa_T$ as $k \to 0$, since $S(0) \sim \kappa_T$ [34]. Third, as can be read off the graphs in Fig. 3, the structure factor exhibits the correct critical exponents as the system approaches either the spinodal curve or the critical point. Finally, by suitably choosing the forcing weights (see Appendix A), it is possible to obtain the same results in one and two dimensions thus facilitating the validation of the theoretical analysis.

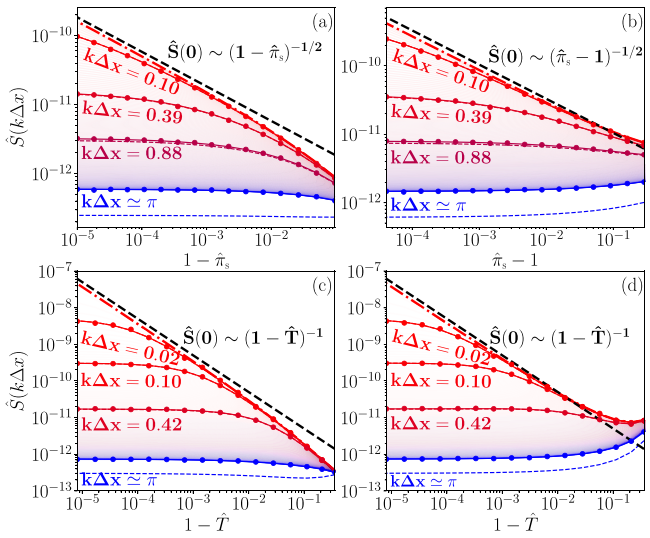


FIG. 3. $S(k)$ as functions of the relative pressure from the spinodal line $|1-\hat{\pi}_s|$ (top), and relative distance from the critical point $1-\hat{T}$ (bottom). Solid lines indicate the analytical prediction, while the dashed lines the truncation to $O(k^2)$. The color scale goes from $k\Delta x = 0$ in red to $k\Delta x = \pi$ in blue (lighter to darker shade). Upon approaching the spinodal line or the critical point the large scale ($k \to 0$ in dot-dashed red) converges to a power-law behavior (in dashed black).

## IV. DISCUSSION AND CONCLUSIONS

All mesoscopic approaches based on a square-gradient free energy [7,8,16] share the same qualitative behavior of $S(k)$ as shown in Fig. 2, i.e., a monotonous decreasing behavior in $k$ which, however, differs from that of liquids at low temperatures [41,42]. The multi-range extension of the SC model [19,31,43,44] may provide a solution: For larger stencils (see Appendix B 3) the denominator of $S(k)$ acquires higher-order contributions, i.e., $\cos(nk)$, providing a Fourier basis to approximate realistic substances. This approach could allow one to continuously change the scale, from the mesoscopic towards the molecular one.

In summary, we studied in this work the metastable and unstable characteristics of the stochastic pseudo-potential lattice Boltzmann model in response to thermal fluctuation. Using a previously obtained pressure tensor, the structure factor is theoretically obtained and numerically verified to high precision. The metastable state is numerically confirmed as stable to small perturbations. Theoretically and numerically, the long-wave-length limit of the structure factor corresponding to the isothermal compressibility is found to diverge with the correct exponents as the system approaches to the spinodal curve or critical point. With the metastable and unstable characteristics quantitatively obtained, the present study paved the way for the pseudo-potential LB model to be used in modeling nucleation taking into hydrodynamic influences as well as a valuable tool in the study of the effects of thermal fluctuations in turbulence [45–47].

All simulations have been run on an architecture-independent GPU/CPU implementation which can be found on the GitHub repository of the "idea.deploy" framework [20–27].


## ACKNOWLEDGMENTS

This work was supported by the National Natural Science Foundation of China Grants No. 12050410244 and No. 92152107, Department of Science and Technology of Guangdong Province Grant No. 2020B1212030001, and Shenzhen Science and Technology Program Grant No. KQTD20180411143441009.


## APPENDIX A: SHAN-CHEN LATTICE BOLTZMANN MODEL

In this Appendix we review the fundamental aspects of the lattice Boltzmann model (LBM) in its usual notation and provide a link to the rescaled notation used in the main text. All LBM equations should be understood as expressed in the so-called *lattice units* [11]. The LBM equation for a system with a local force and stochastic fluctuations can be written as [11,12]

$$f_i(\mathbf{x}+\boldsymbol{\xi}_i, t+1) - f_i(\mathbf{x}, t) = \Omega_i^{(\mathrm{BGK})}(\mathbf{x}, t) + F_i(\mathbf{x}, t) + \eta_i(\mathbf{x}, t). \tag{A1}$$

The collision operator $\Omega_i^{(\mathrm{BGK})}$ can be written as

$$\Omega_i^{(\mathrm{BGK})}(\mathbf{x}, t) = -\frac{1}{\tau}\left[f_i(\mathbf{x}, t) - f_i^{(\mathrm{eq})}(\mathbf{x}, t)\right], \tag{A2}$$

where $\tau$ is the relaxation time and the equilibrium populations $f_i^{(\mathrm{eq})}(\mathbf{x}, t)$ are defined from a second-order approximation of the Maxwell-Boltzmann distribution function

$$f_i^{(\mathrm{eq})}(\mathbf{x}, t) = w_i n\left[1 + \frac{\xi_i^\alpha u_\alpha^{(\mathrm{eq})}}{c_s^2} + \frac{\left(\xi_i^\alpha u_\alpha^{(\mathrm{eq})}\right)^2}{2c_s^4} - \frac{u_\alpha^{(\mathrm{eq})} u_\alpha^{(\mathrm{eq})}}{2c_s^2}\right], \tag{A3}$$

where $c_s^2 = 1/3$ is the square of the sound speed related to the D3Q19 stencil used for the simulations. The equilibrium velocity $u_{(\mathrm{eq})}^\alpha$ is suitably defined to take into account the force term $F^\alpha$ as

$$u_{(\mathrm{eq})}^\alpha(\mathbf{x}, t) = \frac{1}{n(\mathbf{x}, t)} \sum_{i=0}^{N_p-1} \xi_i^\alpha f_i(\mathbf{x}, t) + \frac{1}{2n(\mathbf{x}, t)} F^\alpha(\mathbf{x}, t), \tag{A4}$$

which needs to be paired with the population forcing term [32]

$$F_i = \left(1 - \frac{1}{2\tau}\right) w_i \left[\frac{1}{c_s^2}\xi_i^\alpha + \frac{1}{c_s^4}\left(\xi_i^\alpha \xi_i^\beta - c_s^2 \delta^{\alpha\beta}\right) u_\beta^{(\mathrm{eq})}\right] F_\alpha, \tag{A5}$$

allowing the model to consistently recover all relevant thermodynamic properties [11,12,19]. The density gradients implementing phase separation are triggered by the Shan-Chen (SC) force term [13,14]

$$F^\mu(\mathbf{x}, t) = -G c_s^2 \psi(\mathbf{x}, t) \sum_{a=1}^{18} W(|\mathbf{e}_a|^2) \psi(\mathbf{x}+\mathbf{e}_a, t) e_a^\mu, \tag{A6}$$

with $W(1) = 1/6$ and $W(2) = 1/12$ and $\mathbf{e}_a = \boldsymbol{\xi}_a$ for $a = 1, \ldots, 18$. For multiphase and multicomponent systems the SC model features also a lattice pressure tensor (LPT) [18,19,30,48] that for the three-dimensional model in use

reads

$$P^{\mu\nu}(\mathbf{x},t) = n(\mathbf{x},t)c_s^2\delta^{\mu\nu} + \frac{Gc_s^2}{2}\psi(\mathbf{x},t) \times \sum_{a=1}^{18} W(|\mathbf{e}_a|^2)\psi(\mathbf{x}+\mathbf{e}_a,t)e_a^\mu e_a^\nu. \quad \text{(A7)}$$

As observed in the main text, given that the structure factor $S(k)$ depends only on the *normal* component of the pressure tensor, simulations in one and two dimensions yield the same results when the weights are chosen to be $W(1) = 1/2$ $(d=1)$ and $W(1) = 1/3,\ W(2) = 1/12$ $(d=2)$, respectively. Finally, the random variables $\{\eta_i\}$ are obtained as linear combinations of Gaussian random variables implicitly defined in moment space as $N_a = \sum_i m_{ai}\eta_i$, i.e., $\eta_i = \sum_a (m^{-1})_{ia}N_a$. The details for $m_{ai}$ are provided in Appendix D.

The link with the notation used in the main text is the following: (i) redefine the coupling constant as $-Gc_s^2 \to G > 0$, (ii) substitute the ideal term as $nc_s^2 \to n$, then (iii) normalize the pressure by $G^{-1} = k_BT$ in order to get Eq. (6).

## APPENDIX B: HYDRODYNAMIC FLUCTUATIONS AND MULTIPHASE SC-LBM STRUCTURE FUNCTION

### 1. General formulation

In this section we provide some details about the framework of fluctuating hydrodynamics. More details can be found in [16,17]. The variance for the random stress tensor $R^{\alpha\beta}$ is given in terms of the hydrodynamic fluctuations energy $k_B\vartheta$ by

$$\langle R^{\alpha\beta}(\mathbf{x},t)R^{\mu\nu}(\mathbf{x}',t')\rangle = 2n_0k_B\vartheta\left[\nu_s(\delta^{\alpha\mu}\delta^{\beta\nu}+\delta^{\alpha\nu}\delta^{\beta\mu}) + \left(\nu_b - \frac{2}{d}\nu_s\right)\delta^{\alpha\beta}\delta^{\mu\nu}\right] \times \delta^{(3)}(\mathbf{x}-\mathbf{x}')\delta(t-t'), \quad \text{(B1)}$$

where $\nu_s$ and $\nu_b$ are the shear and bulk kinematic viscosities, respectively [49,50]. In the present case of single relaxation time LBM, Eq. (B1) further simplifies given that the two viscosities are related by $\nu_b = 2\nu_s/d$. The Fourier transform of the linearized Navier-Stokes equations for $\mathbf{u}(\mathbf{x},t) = \delta\mathbf{u}(\mathbf{x},t)$ and $n(\mathbf{x},t) = n_0 + \delta n(\mathbf{x},t)$, read

$$\partial_t\delta\bar{n}(\mathbf{k},t) - \imath n_0k_\alpha\delta\bar{u}^\alpha(\mathbf{k},t) = 0, \quad \text{(B2)}$$

$$\partial_t\delta\bar{u}^\alpha(\mathbf{k},t) = \frac{\imath k_\beta}{n_0}[\delta\bar{P}^{\alpha\beta}(\mathbf{k},t) - \bar{R}^{\alpha\beta}(\mathbf{k},t)] - \nu_s[k^\alpha k_\beta\delta\bar{u}^\beta(\mathbf{k},t) + |\mathbf{k}|^2\delta\hat{u}(\mathbf{k},t)^\alpha] - \left(\nu_b - \frac{2}{d}\nu_s\right)k^\alpha k_\gamma\delta\bar{u}^\gamma(\mathbf{k},t). \quad \text{(B3)}$$

The normalized wave vector $\hat{k}^\alpha = k^\alpha/|\mathbf{k}|$ can be used to project vectors and tensors along the direction *parallel* to $\hat{k}^\alpha$ (indicated by the $||$ subscript) and the *orthogonal* one (indicated by $\perp$). For a generic vector $A^\mu$ or rank-two symmetric tensor $T^{\alpha\beta}$ one can leverage the projector along the orthogonal direction to $\hat{k}^\alpha$, i.e., $q^{\alpha\beta} = \delta^{\alpha\beta} - \hat{k}^\alpha\hat{k}^\beta$, and write

$$A_{||} = A_\mu\hat{k}^\mu, \quad A_\perp^\mu = A_\alpha q^{\alpha\mu}, \quad T_{||} = \hat{k}_\alpha\hat{k}_\beta T^{\alpha\beta}, \quad T_\perp^\alpha = T^{\beta\gamma}\hat{k}_\beta q_\gamma^\alpha. \quad \text{(B4)}$$

We notice that the continuity equation Eq. (B2) is already projected onto the longitudinal velocity while for Eq. (B3) the same projection reads

$$\partial_t\delta\bar{u}_{||}^\alpha(\mathbf{k},t) = \frac{\imath k}{n_0}[\delta\bar{P}_{||}(\mathbf{k},t) - \bar{R}_{||}(\mathbf{k},t)] - \nu_{||}k^2\delta\bar{u}_{||}(\mathbf{k},t) \quad \text{(B5)}$$

with $\nu_{||} = \nu_b + 2(1-1/d)\nu_s$. Now, we focus on the longitudinal projection of the variation of the Fourier-transformed pressure tensor $\delta\bar{P}$. We define the scale-dependent speed of sound $\bar{c}_s^2$ through the relation $\delta\bar{P}_{||}(\mathbf{k},t) = \delta\bar{P}^{\mu\nu}(\mathbf{k},t)\hat{k}_\mu\hat{k}_\nu = \bar{c}_s^2(k)\delta\bar{n}(\mathbf{k},t)$. One can make use of Eq. (B2) and solve for the longitudinal velocity as $\delta\bar{u}_{||}(\mathbf{k},t) = -\imath\,\partial_t\delta\bar{n}(\mathbf{k},t)/n_0k$, which can be plugged into Eq. (B5), thus yielding a second-order equation in time for $\delta\hat{n}$,

$$\left[\partial_t^2 + \nu_{||}k^2\partial_t + k^2\bar{c}_s^2(k)\right]\delta\bar{n}(\mathbf{k},t) = -k^2\bar{R}_{||}(\mathbf{k},t), \quad \text{(B6)}$$

which, after a Fourier transform in the time domain, can be used to express $\delta\bar{n}(\omega,\mathbf{k})$ as

$$\delta\bar{n}(\mathbf{k},\omega) = \frac{k^2\bar{R}_{||}(\mathbf{k},\omega)}{\omega^2 - k^2\bar{c}_s^2(k) + \imath\,\nu_{||}k^2\omega}, \quad \text{(B7)}$$

thus yielding the dynamic structure factor as $S(\mathbf{k},\omega) = \langle|\delta\hat{n}(\mathbf{k},\omega)|^2\rangle$. Considering that $\langle|\bar{R}_{||}(k,t)|^2\rangle = 2n_0k_B\vartheta\,\nu_{||}$, one can perform a contour integration over complex values of $\omega$ and obtain the general expression for the static structure factor

$$\bar{S}(k) = \frac{n_0k_B\vartheta}{\bar{c}_s^2(k)}. \quad \text{(B8)}$$

The specific expression of $\bar{c}_s^2(k)$ depends on the underlying model used for phase separation.

### 2. Multiphase Shan-Chen model

We begin by rewriting the lattice pressure tensor [19,30,31]

$$P^{\mu\nu}(\mathbf{x},t) = n(\mathbf{x},t)k_BT\delta^{\mu\nu} - \frac{1}{2}\psi(\mathbf{x},t) \times \sum_{i=0}^{18} W(|\boldsymbol{\xi}_i|^2)\psi(\mathbf{x}+\boldsymbol{\xi}_i,t)\xi_i^\mu\xi_i^\nu. \quad \text{(B9)}$$

When taking the spatial Fourier transform, the unit vector $\hat{k}^\mu$ lies along the direction of the density gradient $\partial^\mu\delta n$, so that when we consider the variation of the longitudinal projection of the pressure tensor, i.e., $\delta\hat{P}_{||} = \delta\hat{P}^{\mu\nu}\hat{k}_\mu\hat{k}_\nu$, one is actually selecting the normal component of the pressure tensor $P_N$ with respect to the gradient of the local density fluctuations. Without loss of generality, one can assume $\hat{k} = \hat{x}$, so that $P_N = P^{xx}$ which from Eq. (B9) follows as

$$P_N(x) = n(x)k_BT - \tfrac{1}{4}\psi(x)[\psi(x+1) + \psi(x-1)]. \quad \text{(B10)}$$

As shown in Fig. 4, the expression above enjoys the fundamental property of yielding a constant value, up to machine precision, when evaluated across a flat interface [19,31], i.e., $P_N = P_0$. This represents an exact implementation on the discrete lattice of the *mechanic equilibrium* condition [51], i.e., any normal pressure gradient, even through the interface, would cause the latter to move. It is possible to show that the finite difference $[P_N(x+1) - P_N(x-1)]/2 = 0$ coincides

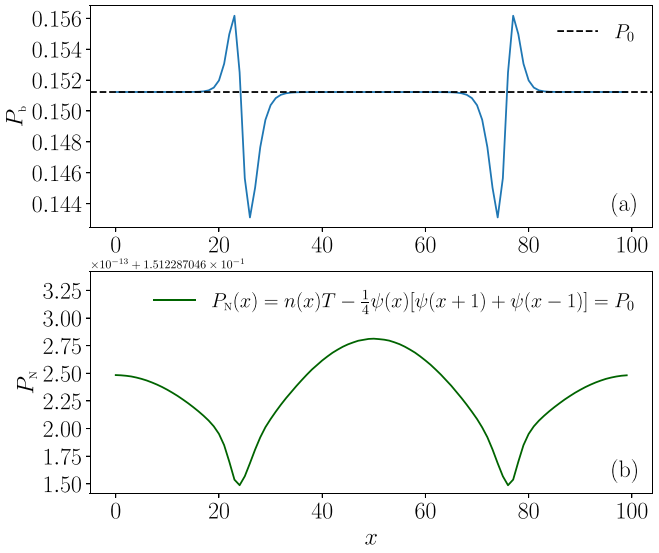


FIG. 4. (a) Flat interface bulk pressure profile $P_b = n(x)T - \psi^2(x)/2$, the bulk pressure value $P_0$ is consistently obtained in both phases away from the interface. (b) Lattice pressure tensor normal component, displaying fluctuations of the order of $10^{-13}$, i.e., constant to machine precision. Results are expressed in *lattice units* [11].

with a linear combination of the forced lattice Boltzmann equations at stationarity [52]. We can equivalently express Eq. (B10) in terms of its Taylor expansion as

$$P_{\rm N}(x) = \left[n(x)k_BT - \frac{1}{2}\psi^2(x)\right] - \frac{1}{2}\psi(x)\sum_{n=1}^{+\infty}\frac{1}{(2n)!}\frac{d^{2n}}{dx^{2n}}\psi(x),$$

of which we can take the variation with respect to the density fluctuations as

$$\delta P_{\rm N}(x) = [k_BT - \psi_0\psi_0']\delta n(x) - \frac{1}{2}\psi_0\psi_0'\sum_{n=1}^{+\infty}\frac{1}{(2n)!}\frac{d^{2n}}{dx^{2n}}\delta n(x).$$

Finally, by taking the Fourier transform of the equation, and defining $\bar{c}_{s,0}^2 = k_BT - \psi_0\psi_0'$, we obtain

$$\delta\bar{P}_{\rm N}(k) = \left[\bar{c}_{s,0}^2 - \frac{1}{2}\psi_0\psi_0'\sum_{n=1}^{+\infty}\frac{(-)^n}{(2n)!}k^{2n}\right]\delta\bar{n}(k). \tag{B11}$$

Now, we wish to compute the adimensional form of this expression. In this respect, we normalize the pressure variation by the critical pressure $P_c = n_ck_BT_c/2$ and multiply $k$ by the lattice spacing $\Delta x$ thus yielding

$$\delta\hat{P}_{\rm N}(k\Delta x) = \left[\frac{2\bar{c}_{s,0}^2}{k_BT_c} - \frac{1}{k_BT_c}\psi_0\psi_0'\sum_{n=1}^{+\infty}\frac{(-)^n}{(2n)!}(k\Delta x)^{2n}\right]\delta\hat{n}(k). \tag{B12}$$

For the pseudo-potential we are considering $\psi = \exp(-1/n)$ one has that $k_BT_c = e^{-2}$. Hence, we redefine $e\psi \to \psi$ so that we write

$$\delta\hat{P}_{\rm N}(k\Delta x) = \left[\hat{c}_{s,0}^2 - \psi_0\psi_0'\sum_{n=1}^{+\infty}\frac{(-)^n}{(2n)!}(k\Delta x)^{2n}\right]\delta\hat{n}(k) \tag{B13}$$

with $\hat{c}_{s,0}^2 = 2\hat{T} - 2\psi_0\psi_0'$. We notice that the series can be summed finally yielding the exact expression

$$\hat{c}_s^2(k\Delta x) = \hat{c}_{s,0}^2 - \psi_0\psi_0'[\cos(k\Delta x) - 1]. \tag{B14}$$

We can relate the above expression to its dimensionalized form as $\bar{c}_s^2 = k_BT_c\hat{c}_s^2/2$, and notice that in order to recast Eq. (B8) in nondimensional form one can normalize it by $n_c^2$, hence one gets

$$\hat{S}(k\Delta x) = \frac{1}{n_c^2}\frac{2n_0k_B\vartheta}{k_BT_c\hat{c}_s^2(k\Delta x)} = \frac{2\hat{n}_0\hat{\vartheta}}{n_c\hat{c}_s^2(k\Delta x)} \tag{B15}$$

from which one can compute the full expression for the SC multiphase model as

$$\hat{S}(k\Delta x) = 2\hat{n}_0\hat{\vartheta}/n_c\left\{\hat{c}_{s,0}^2 - \psi_0\psi_0'[\cos(k\Delta x) - 1]\right\}. \tag{B16}$$

In [16] a free-energy model was adopted and the results were later extended to the Shan-Chen model in [17] where $\bar{c}_s^2(k)$ was approximated up to $O(k^2)$. A mismatch ($\gtrsim$15%) between the numerical values of the structure factor $S(k)$ and its theoretical expression were reported in [17]. The latter may be due to (i) the low approximation order and (ii) the use of an approximate expression for the pressure tensor derived from the Taylor expansion of the force in Eq. (A6) rather than the lattice version Eq. (A7).

As discussed in the main text, it is possible to rearrange the terms and obtain a direct mapping onto the functional form of the momentum-space propagator of the Gaussian Ising model [36]. For the expression in lattice units [11] one obtains

$$G_0(k) = \frac{S(k)}{n_0k_B\vartheta}\left(c_s^2 + \frac{1}{2}\psi_0\psi_0'\right) = \frac{1}{1 - 2\beta\cos(k)}, \tag{B17}$$

with the inverse temperature defined as

$$2\beta = \frac{\psi_0\psi_0'/2}{T + \psi_0\psi_0'/2} = \frac{1}{1 + 2/(\psi_0\psi_0')} > 0. \tag{B18}$$

### 3. Multibelt extension

The extension of the Shen-Chen interaction potential to stencils including points farther away than those considered in Eq. (A6) has been thoroughly analyzed in a series of works [19,29,31,44,53–55]. The main feature is that of the introduction of new vectors subgroups related to new forcing stencil weights $W$ which in turn can be used to implement higher order isotropy conditions or to tune physical properties such as surface tension independently. Given that the structure factor $S(k)$ entirely depends on the form of the normal component of the pressure tensor Eq. (B10), one can use the expression of the 12th-order isotropic stencil [Eqs. (D4) and (D5) in [19]] and find the normalized structure factor to be

$$\bar{S}(k\Delta x) = \frac{S(k\Delta x)}{k_B\vartheta}c_s^2 = \frac{1}{1 + 2G\psi_0\psi_0'\left[\sum_{n=0}^{4}c_n\cos(nk\Delta x)\right]}, \tag{B19}$$

where the coefficients $c_n$ are defined, following the notation for the pressure tensor coefficients in [19], as

$$\begin{aligned} c_0 &= a^{(N)}_{[-1,0,1]} + a^{(N)}_{[-2,0,2]} + a^{(N)}_{[-3,0,3]} + a^{(N)}_{[-4,0,4]} \\ c_1 &= a^{(N)}_{[-1,0,1]} + b^{(N)}_{[1,1]} + b^{(N)}_{[1,2]} + b^{(N)}_{[1,3]} \\ c_2 &= a^{(N)}_{[-2,0,2]} + b^{(N)}_{[1,2]} + b^{(N)}_{[2,2]} \\ c_3 &= a^{(N)}_{[-3,0,3]} + b^{(N)}_{[1,3]} \\ c_4 &= a^{(N)}_{[-4,0,4]}. \end{aligned} \tag{B20}$$

One can prove that $c_0 - c_1 + c_2 - c_3 + c_4 = 0$, hence the large-$k$ limit of $\bar{S}(k)$ is unity as expected:

$$\bar{S}(k\Delta x)|_{k\Delta x=\pi} = \frac{1}{1 + 2G\psi_0\psi_0'[c_0 - c_1 + c_2 - c_3 + c_4]} = 1. \tag{B21}$$

In order to obtain $\bar{S}(k)$ with real substances features one can impose the value of $\bar{S}(0) < 1$ as

$$\bar{S}(k\Delta x)|_{k=0} = \frac{1}{1 + 2G\psi_0\psi_0'[c_0 + c_1 + c_2 + c_3 + c_4]} < 1, \tag{B22}$$

and the derivative at $k = 0$ to be positive,

$$\left[\frac{d\bar{S}(k\Delta x)}{dk}\right]_{k\simeq 0} \propto 2G\psi_0\psi_0'(c_1 + 4c_2 + 9c_3 + 16c_4)k > 0. \tag{B23}$$

These conditions need to be set with a specific choice of the pseudo-potential, i.e., of an equation of state allowing one to satisfy both Eqs (B22) and (B23). This can be obtained with the Carnahan-Starling equation of state [56]

$$p = nRT\left[\frac{1 + bn/4 + (bn/4)^2 - (bn/4)^3}{(1 - bn/4)^3}\right] - an^2, \tag{B24}$$

where one can fix the parameters in terms of the critical parameters [57]

$$\begin{aligned} a &\simeq \frac{1.38\,286\,523\,464\,159RT_c}{n_c}, \\ b &\simeq \frac{0.521\,775\,536\,769\,816}{n_c}, \end{aligned} \tag{B25}$$

and we select the critical parameters as $n_c = \log(2)$ and $P_c \simeq 0.358\,956\,205\,778\,117RT_cn_c$ with $P_c = n_c(1 - 1/2\log 2)/3$, thus matching the values that are obtained for the choice $\psi = 1 - \exp(-n)$. It is possible to choose the parameter values (see Table I) for the stencil such that the conditions (B22) and (B23) are satisfied in a reasonably large temperature range. The results reported in Fig. 5 display the characteristic features, oscillations and their amplitude as a function of temperature, observed in both real and ideal systems [41,58].

## APPENDIX C: ISOTHERMAL ASSUMPTION AND HEAT DISSIPATION

In order to assess the validity of the isothermal assumption in the present treatment, it is interesting to compute the energy provided by the stress tensor and dissipated by the system. We can write the stress tensor and the pressure tensor as

$$\begin{aligned} \sigma^{\alpha\beta}(\mathbf{x},t) &= c_s^2\left(\tau - \tfrac{1}{2}\right)n_0[\partial^\alpha \delta u^\beta(\mathbf{x},t) + \partial^\beta \delta u^\alpha(\mathbf{x},t)] \\ &\quad + R^{\alpha\beta}(\mathbf{x},t), \\ P^{\alpha\beta} &= c_s^2[n_0 + \delta n(\mathbf{x},t)]\delta^{\alpha\beta} + \delta P_{\mathrm{I}}^{\alpha\beta}(\mathbf{x},t). \end{aligned} \tag{C1}$$

The work per unit time done by the fluctuations can be written as

$$\begin{aligned} w = \frac{W}{\Lambda} \simeq \Big\langle \int d^D x \big[ &-c_s^2[n_0 + \delta n(\mathbf{x})]\delta^{\alpha\beta} - \delta P_{\mathrm{I}}^{\alpha\beta}(\mathbf{x}) \\ &+ \sigma^{\alpha\beta}(\mathbf{x})\big]\partial_\alpha \delta u_\beta(\mathbf{x})\Big\rangle, \end{aligned} \tag{C2}$$

TABLE I. Weights for the stencil yielding the oscillatory behavior of the structure factor using the Carnahan-Starling equation of state [56] reported in Fig. 5.

| | |
|---|---|
| $W(1)$ | $-52\,397\,848\,003/162\,108\,928\,800$ |
| $W(2)$ | $2\,269\,960\,703/10\,131\,808\,050$ |
| $W(4)$ | $107\,580\,263/890\,708\,400$ |
| $W(5)$ | $-7\,645\,065\,671/64\,843\,571\,520$ |
| $W(8)$ | $285\,804\,161/4\,156\,639\,200$ |
| $W(9)$ | $-1\,098\,810\,131/162\,108\,928\,800$ |
| $W(10)$ | $57\,890\,947/1\,621\,089\,288$ |
| $W(13)$ | $-378\,977\,623/108\,072\,619\,200$ |
| $W(16)$ | $109\,121\,669/81\,054\,464\,400$ |
| $W(17)$ | $-298\,631\,969/162\,108\,928\,800$ |

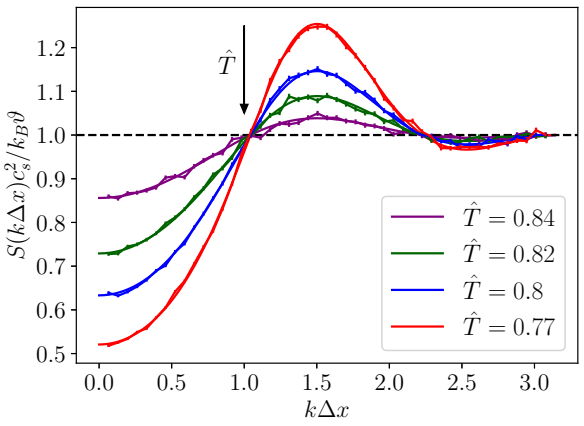


FIG. 5. Normalized static density structure function $S(k)$ for the Carnahan-Starling equation of state implemented with the Shan-Chen multiphase approach. The forcing stencil has been tuned in such a way that at low temperature $S(k)$ displays similar features to that of realistic fluids: (1) $\bar{S}(0) < 1$, (2) $d\bar{S}/dk|_{k=0} > 0$, and (3) oscillations around 1 as the limit $k \to \pi$ is approached. The peak of the decreases as the temperature increases as indicated by the arrow. This procedure can be understood as the result of the coarse graining of the molecular properties of a liquid at a given scale. Results are expressed in *lattice units* [11].

TABLE II. The set of polynomials $m_{ai}$ used for the projection onto moment space, obtained from the Gram-Schmidt procedure applied onto a set of Hermite polynomials, the respective weighted *norm* $M_{ai}$, and the stencil weights $w_i$ and the associated stencil vector $\boldsymbol{\xi}_i$.

| $(a,i)$ | $m_{ai}$ | $M_a$ | $w_i$ | $\boldsymbol{\xi}_i$ |
|---|---|---|---|---|
| 0 | $1$ | 1 | 1/3 | (0, 0, 0) |
| 1 | $\xi_i^x$ | 1/3 | 1/18 | (1, 0, 0) |
| 2 | $\xi_i^y$ | 1/3 | 1/18 | (0, 1, 0) |
| 3 | $\xi_i^z$ | 1/3 | 1/18 | (−1, 0, 0) |
| 4 | $(\xi_i^x)^2 - \frac{1}{3}$ | 2/9 | 1/18 | (0, −1, 0) |
| 5 | $\xi_i^x \xi_i^y$ | 1/9 | 1/18 | (0, 0, 1) |
| 6 | $\xi_i^x \xi_i^z$ | 1/9 | 1/18 | (0, 0, −1) |
| 7 | $(\xi_i^y)^2 - \frac{1}{3}$ | 2/9 | 1/36 | (1, 1, 0) |
| 8 | $\xi_i^y \xi_i^z$ | 1/9 | 1/36 | (−1, 1, 0) |
| 9 | $(\xi_i^z)^2 - \frac{1}{3}$ | 2/9 | 1/36 | (−1, −1, 0) |
| 10 | $\xi_i^y((\xi_i^x)^2 - \frac{1}{3})$ | 2/27 | 1/36 | (1, −1, 0) |
| 11 | $\xi_i^z((\xi_i^x)^2 - \frac{1}{3})$ | 2/27 | 1/36 | (1, 0, 1) |
| 12 | $\xi_i^x((\xi_i^y)^2 - \frac{1}{3})$ | 2/27 | 1/36 | (−1, 0, 1) |
| 13 | $\frac{1}{2}\xi_i^x((\xi_i^y)^2 + 2(\xi_i^z)^2 - 1)$ | 1/18 | 1/36 | (−1, 0, −1) |
| 14 | $\frac{1}{2}\xi_i^z((\xi_i^x)^2 + 2(\xi_i^y)^2 - 1)$ | 1/18 | 1/36 | (1, 0, −1) |
| 15 | $\frac{1}{2}\xi_i^y((\xi_i^x)^2 + 2(\xi_i^z)^2 - 1)$ | 1/18 | 1/36 | (0, 1, 1) |
| 16 | $(\xi_i^x)^2(\xi_i^y)^2 - \frac{1}{3}(\xi_i^x)^2 - \frac{1}{3}(\xi_i^y)^2 + \frac{1}{6}(\xi_i^z)^2 + \frac{1}{18}$ | 7/162 | 1/36 | (0, −1, 1) |
| 17 | $\frac{2}{7}(\xi_i^x)^2(\xi_i^y)^2 + (\xi_i^x)^2(\xi_i^z)^2 - \frac{3}{7}(\xi_i^x)^2 + \frac{1}{14}(\xi_i^y)^2 - \frac{2}{7}(\xi_i^z)^2 + \frac{1}{14}$ | 5/126 | 1/36 | (0, −1, −1) |
| 18 | $\frac{2}{5}(\xi_i^x y)^2(\xi_i^y)^2 + \frac{2}{5}(\xi_i^x)^2(\xi_i^z)^2 - \frac{1}{10}(\xi_i^x)^2 + (\xi_i^y)^2(\xi_i^z)^2 - \frac{2}{5}(\xi_i^y)^2 - \frac{2}{5}(\xi_i^z)^2 + \frac{1}{10}$ | 1/30 | 1/36 | (0, 1, −1) |

where $\Lambda$ is the duration of the time interval. We write now this quantity in Fourier space

$$w = \frac{W}{\Lambda} \simeq \left\langle \int \frac{d^D k}{(2\pi)^D} \left[ -c_s^2 [n_0 + \delta\hat{n}(\mathbf{k})]\delta^{\alpha\beta} - \delta\hat{P}_1^{\alpha\beta}(\mathbf{k}) + \hat{\sigma}^{\alpha\beta}(\mathbf{k}) \right] (\imath k_\alpha)\delta\hat{u}_\beta(-\mathbf{k}) \right\rangle$$
$$= c_s^2 \left(\tau - \frac{1}{2}\right) n_0 \int \frac{d^D k}{(2\pi)^D} [k^2 \langle |\delta\hat{u}_\parallel(\mathbf{k})|^2\rangle + Dk^2 \langle |\delta\hat{u}(\mathbf{k})|^2\rangle]. \tag{C3}$$

Here we considered that for a homogeneous quiescent state one has $\langle \delta u \rangle = 0$, which in turn implies $\langle \partial \delta u \rangle = 0$. Further, it is possible to show that $\langle \delta n(\mathbf{k}) \delta u(-\mathbf{k}) \rangle = \frac{1}{2\pi} \int d\omega \langle \delta n(\mathbf{k}, \omega) \delta u(-\mathbf{k}, -\omega) \rangle = 0$ so that also the terms proportional to $\langle \delta \hat{P}_1 \partial \delta u \rangle$ vanish, given that $\delta \hat{P}_1 \propto \delta \hat{n}$. Finally, we make use of the nonanticipating character of all the hydrodynamic fluctuations with respect to the noise and set $\langle R \partial \delta u \rangle = 0$. Hence, after considering the velocity structure factor to be $\langle |\hat{u}^\alpha(k)|^2 \rangle = \langle |\hat{u}_\parallel(k)|^2 \rangle = k_B \vartheta / n_0$ we write

$$w = \frac{W}{\Lambda} \simeq c_s^2 \left(\tau - \frac{1}{2}\right) k_B \vartheta (1 + D) \int \frac{d^D k}{(2\pi)^D} k^2. \tag{C4}$$

The above expression for $w$ is always of order $O(k_B\vartheta)$ so that, if normalized by the volume $V(\Omega)$ would yield a vanishing result in the thermodynamic limit, i.e., any local nonequilibrium $\delta T$ would be very small. This result is in agreement with the observations reported in [35].

## APPENDIX D: LBM SIMULATIONS

### 1. Population noise variance

As detailed in [17] one needs only to specify the variance of the noise moments $N_a = \sum_i m_{ai} \eta_i$, where $\eta_i$ is the population noise appearing in the stochastic LB equation (A2). In order to guarantee exact conservation of density and momentum, one needs to set the variance of the related stochastic moments to zero, i.e., ordering the moments as reported in Table II one can write a diagonal covariance matrix as follows:

$$\Xi_{ab} = \langle N_a N_b \rangle = \frac{n_0 k_B \vartheta}{c_s^2} \frac{1}{\tau} \left(2 - \frac{1}{\tau}\right) \mathrm{diag}[0, 0, 0, 0, M_4, \ldots, M_{18}], \tag{D1}$$

where $M_a = \sum_i w_i m_{ai}^2$ represents the *norm* of the moments over the weighted scalar product in the population space. Equation (D1) implies that all the stochastic moments are simply uncorrelated Gaussian random numbers that can be independently computed via a Box-Müller transform [59] starting from two uniformly distributed pseudo-random numbers. The most important property of the moments $m_{ai}$ is their orthogonality with respect to the weighted scalar product in population space, i.e., $\delta_{ab} = \sum_i w_i m_{ai} m_{bi}$. While for the two-dimensional case it is enough to consider a basis given by Hermite polynomials, in three dimensions this is no longer possible because of the nonhydrodynamic higher-order ghost moments [11,12]. Hence, we resorted to the Gram-Schmidt orthogonalization over some set of three-dimensional Hermite polynomial yielding the results reported in Table II.

### 2. Data analysis

The discrete Fourier transform are performed in a straightforward way as described in the definition of the Fourier transform for the spin-glass susceptibility in [60]. Given that $S(k)$ depends only on the norm of $\mathbf{k}$ and that it is given by the complex norm of $\delta n(k)$ then one can average the results obtained along the three directions,

$$\mathbf{k}_x = (k, 0, 0), \quad \mathbf{k}_y = (0, k, 0), \quad \mathbf{k}_z = (0, 0, k), \tag{D2}$$

and simply compute the squared norm as

$$|\delta\hat{n}_x(k,t)|^2 = \frac{1}{L}\sum_x \{[\delta n_{yz}(x)\cos(kx)]^2 + [\delta n_{yz}(x)\sin(kx)]^2\}, \tag{D3}$$

where we defined the plane average as

$$\delta n_{yz}(x) = \frac{1}{L^2}\sum_{y,z}\delta n(x,y,z). \tag{D4}$$

One can repeat the computation for the three different direction for a sequence of time values $t = 1, \ldots, T$ and obtain the steady-state average as

$$\langle|\delta\hat{n}(k)|^2\rangle = \frac{1}{T}\sum_{t=1}^{T}\frac{1}{3}[|\delta n_x(k,t)|^2 + |\delta n_y(k,t)|^2 + |\delta n_z(k,t)|^2]. \tag{D5}$$

The values for $\cos(kx)$ and $\sin(kx)$ can be stored in look-up tables for each value of $k = 2\pi n_k/L$ with $n_k = 1, \ldots, \lfloor L/2 \rfloor$, thus computing them only once.


[1] P. G. Debenedetti, *Metastable Liquids: Concepts and Principles* (Princeton University Press, Princeton, NJ, 1996).
[2] V. I. Kalikmanov, in *Nucleation Theory*, Lecture Notes in Physics, Vol. 860, edited by W. Beiglböck, J. Ehlers, K. Hepp, and H. Weidenmüller (Springer, Netherlands, Dordrecht, 2013), pp. 37–187.
[3] C. E. Brennen, *Fundamentals of Multiphase Flow* (Cambridge University Press, Cambridge, 2005).
[4] D. Lohse and A. Prosperetti, Proc. Natl. Acad. Sci. USA **113**, 13549 (2016).
[5] L. D. Landau, E. M. Lifshitz, and R. T. Beyer, *Perspectives in Theoretical Physics - The Collected Papers of E. M. Lifshitz* (Pergamon, Amsterdam, Elsevier, 1992), pp. 359–361.
[6] J. S. Rowlinson and B. Widom, *Molecular Theory of Capillarity* (Dover Publications, Mineola, NY, 1982).
[7] A. Chaudhri, J. B. Bell, A. L. Garcia, and A. Donev, Phys. Rev. E **90**, 033014 (2014).
[8] M. Gallo, F. Magaletti, and C. M. Casciola, Phys. Rev. Fluids **3**, 053604 (2018).
[9] F. Magaletti, M. Gallo, and C. M. Casciola, Sci. Rep. **11**, 20801 (2021).
[10] M. te Vrugt, H. Löwen, and R. Wittkowski, Adv. Phys. **69**, 121 (2020).
[11] T. Krüger, H. Kusumaatmaja, A. Kuzmin, O. Shardt, G. Silva, and E. M. Viggen, *The Lattice Boltzmann Method* (Springer, Switzerland, 2017).
[12] S. Succi, *The Lattice Boltzmann Equation: For Complex States of Flowing Matter* (Oxford University Press, Oxford, 2018).
[13] X. Shan and H. Chen, Phys. Rev. E **47**, 1815 (1993).
[14] X. Shan and H. Chen, Phys. Rev. E **49**, 2941 (1994).
[15] K. Binder, B. J. Block, P. Virnau, and A. Tröster, Am. J. Phys. **80**, 1099 (2012).
[16] M. Gross, R. Adhikari, M. E. Cates, and F. Varnik, Phys. Rev. E **82**, 056714 (2010).
[17] M. Gross, R. Adhikari, M. E. Cates, and F. Varnik, Philos. Trans. R. Soc. A **369**, 2274 (2011).
[18] M. Sbragaglia and D. Belardinelli, Phys. Rev. E **88**, 013306 (2013).
[19] M. Lulli, L. Biferale, G. Falcucci, M. Sbragaglia, and X. Shan, Phys. Rev. E **103**, 063309 (2021).
[20] https://github.com/lullimat/idea.deploy.
[21] P. Virtanen, R. Gommers, T. E. Oliphant, M. Haberland, T. Reddy, D. Cournapeau, E. Burovski, P. Peterson, W. Weckesser, J. Bright *et al.*, Nat. Methods **17**, 261 (2020).
[22] T. E. Oliphant, *A Guide to NumPy* (Trelgol Publishing, USA, 2006), Vol. 1.
[23] S. Van Der Walt, S. C. Colbert, and G. Varoquaux, Comput. Sci. Eng. **13**, 22 (2011).
[24] F. Pedregosa, G. Varoquaux, A. Gramfort, V. Michel, B. Thirion, O. Grisel, M. Blondel, P. Prettenhofer, R. Weiss, V. Dubourg *et al.*, J. Mach. Learn. Research **12**, 2825 (2011).
[25] J. D. Hunter, Comput. Sci. Eng. **9**, 90 (2007).
[26] F. Pérez and B. E. Granger, Comput. Sci. Eng. **9**, 21 (2007).
[27] A. Klöckner, N. Pinto, Y. Lee, B. Catanzaro, P. Ivanov, and A. Fasih, Parallel Comput. **38**, 157 (2012).
[28] X. Shan and X. He, Phys. Rev. Lett. **80**, 65 (1998).
[29] X. Shan, X.-F. Yuan, and H. Chen, J. Fluid Mech. **550**, 413 (2006).
[30] X. Shan, Phys. Rev. E **77**, 066702 (2008).
[31] M. Sbragaglia, R. Benzi, L. Biferale, S. Succi, K. Sugiyama, and F. Toschi, Phys. Rev. E **75**, 026702 (2007).
[32] Z. Guo, C. Zheng, and B. Shi, Phys. Rev. E **65**, 046308 (2002).
[33] J. L. Thomas, D. J. Tobias, and A. D. MacKerell, J. Phys. Chem. B **111**, 12941 (2007).
[34] V. I. Kalikmanov, *Statistical Physics of Fluids: Basic Concepts and Applications*, Texts and Monographs in Physics (Springer, Berlin, 2001).
[35] M. Gross, Thermal fluctuations in non-ideal fluids with the Lattice Boltzmann method, Ph.D. thesis, Ruhr-Universität Bochum, 2012.
[36] G. Parisi, *Statistical Field Theory* (Avalon Publishing, CA, USA, 1998).
[37] Lbu stands for lattice Boltzmann units, given that we are not matching a specific physical system. The order of magnitude of $k_B\vartheta$ is compatible with the previous LBM literature [16,17].
[38] A. Tröster and K. Binder, Phys. Rev. Lett. **107**, 265701 (2011).
[39] R. C. Tolman, J. Chem. Phys. **17**, 333 (1949).
[40] M. Lulli, L. Biferale, G. Falcucci, M. Sbragaglia, and X. Shan, Phys. Rev. E **105**, 015301 (2022).
[41] G. N. Clark, C. D. Cappa, J. D. Smith, R. J. Saykally, and T. Head-Gordon, Mol. Phys. **108**, 1415 (2010).
[42] A. H. Narten and H. A. Levy, J. Chem. Phys. **55**, 2263 (1971).
[43] X. Shan, Phys. Rev. E **73**, 047701 (2006).

[44] G. Falcucci, G. Bella, G. Chiatti, S. Chibbaro, M. Sbragaglia, and S. Succi, Commun. Comput. Phys. **2**, 1071 (2007).
[45] J. B. Bell, A. Nonaka, A. L. Garcia, and G. Eyink, J. Fluid Mech. **939**, A12 (2022).
[46] R. M. McMullen, M. C. Krygier, J. R. Torczynski, and M. A. Gallis, Phys. Rev. Lett. **128**, 114501 (2022).
[47] Q. Ma, C. Yang, S. Chen, K. Feng, and J. Zhang, Adv. Aerodyn. **5**, 3 (2023).
[48] C. S. From, E. Sauret, S. A. Galindo-Torres, and Y. T. Gu, Phys. Rev. E **99**, 063318 (2019).
[49] L. Landau, E. Lifshitz, and R. Beyer, in *Perspectives in Theoretical Physics* (Elsevier, Amsterdam, Netherlands, 1992), pp. 359–361.
[50] L. P. Pitaevskii and E. M. Lifshitz, *Statistical Physics, Part 2: Volume 9 (Course of Theoretical Physics Vol. 9)* (Butterworth-Heinemann, Oxford, UK, 1980).
[51] J. S. Rowlinson, J. Phys. A: Math. Gen. **17**, L357 (1984).
[52] M. Lulli, C. Coreixas, F. Pelusi, G. Falcucci, M. Sbragaglia, D. Yang, and X. Shan (unpublished).
[53] Q. Li and K. H. Luo, Phys. Rev. E **88**, 053307 (2013).
[54] Q. Li, K. Luo, Q. Kang, Y. He, Q. Chen, and Q. Liu, Prog. Energy Combust. Sci. **52**, 62 (2016).
[55] S. Hosseini, B. Dorschner, and I. Karlin, J. Fluid Mech. **953**, A4 (2022).
[56] N. F. Carnahan and K. E. Starling, J. Chem. Phys. **51**, 635 (1969).
[57] S. S. Baakeem, S. A. Bawazeer, and A. Mohamad, Int. J. Multiphase Flow **128**, 103290 (2020).
[58] B. Cichocki and B. U. Felderhof, J. Chem. Phys. **98**, 8186 (1993).
[59] G. E. P. Box and M. E. Muller, Ann. Math. Stat. **29**, 610 (1958).
[60] M. Lulli, G. Parisi, and A. Pelissetto, Phys. Rev. E **93**, 032126 (2016).